Synthetic Metals 160 (2010) 1654–1661

Contents lists available at ScienceDirect

Synthetic Metals

journal homepage: www.elsevier.com/locate/synmet

Investigation of new PPV-type polymeric materials containing fluorene and thiophene units and their application in organic solar cells

Jilian Nei de Freitas[a], Almantas Pivrikas[b], Bruno F. Nowacki[c], Leni C. Akcelrud[c], N. Serdar Sariciftci[b], Ana Flávia Nogueira[a,*]

[a] Laboratório de Nanotecnologia e Energia Solar (LNES), Universidade Estadual de Campinas (UNICAMP), P.O. Box 6154, 13083-970 Campinas, SP, Brazil
[b] Linz Institute for Organic Solar Cells (LIOS), Johannes Kepler University Linz, Altenberger Strasse 69, A-4040 Linz, Austria
[c] Laboratório de Polímeros Paulo Scarpa (LaPPS), Universidade Federal do Paraná, UFPR, Curitiba, Brazil

ARTICLE INFO

Article history:
Received 28 January 2010
Received in revised form 23 April 2010
Accepted 28 May 2010
Available online 25 June 2010

Keywords:
Conducting polymers
PPV
Polyfluorene
Polythiophene
Organic solar cells

ABSTRACT

New poly(*p*-phenylenevinylene) (PPV)-type conducting polymers containing different concentrations of thiophene and fluorene functional units were investigated in this work and the photophysical and electrochemical properties were evaluated. We observed a dependence of these properties on the concentration of thiophene units in the polymer backbone. The hole mobilities were estimated to be on the order of 10^{-6} cm^2 V^{-1} s^{-1}. The polymers were combined with different concentrations of a soluble fullerene derivative (PCBM) and applied in bulk-heterojunction photovoltaic cells. The effects of PCBM concentration and of annealing (post-production treatment) on these devices were investigated. The best results were obtained for the materials containing higher concentrations of thiophene units.

1. Introduction

Organic solar cells are among the most promising devices for low cost solar energy conversion. In these devices, the polymeric materials are important components, acting as light absorbers, electron donors and hole transporters. Fullerene acts as an electron acceptor and transporter. The introduction of a post-production treatment (annealing), the addition of small alkyl thiol molecules, the optimization of solvent conditions and device design improved the power conversion efficiency of these devices [1–5]. Although remarkable progress has been made in device efficiency in the last few years, important bottlenecks, including nanomorphology, mismatches with the solar spectrum, adjustments of the highest occupied molecular orbital (HOMO) energies of the semiconducting polymers (which affect the open circuit voltage), and stability, still remain to be improved.

Conjugated polymers are important materials for the development of a variety of advanced optical and electronic applications (light emitting diodes, photovoltaic cells, field effect transistors and non-linear optical materials). Among the most used polymers in optoelectronic devices are the poly(*p*-phenylenevinylene)s (PPV), polyfluorenes, polythiophenes and their derivatives. The insertion of side-chains in these polymers reduces the rigidity of the backbone, increases their solubility and enables the preparation of films through inexpensive, solution-based methods, such as casting and spin-coating [6]. Besides, these ramifications can also be used to tune the photophysical and electrochemical properties of these polymers using a variety of routes. For example, the modification of PPV with alkoxy side-chains made possible the synthesis of the polymer poly[2-methoxy-5-(3,7-dimethyloctyloxy)-*p*-phenylene vinylene] (MDMO-PPV), which presents an absorption maximum at 500 nm, while the unmodified PPV presents its absorption maximum at 420 nm [7]. This change in properties allowed the use of MDMO-PPV in organic solar cells with 2.5% of efficiency [8].

Poly(fluorenevinylene)s have similar structures to PPV. In these materials, the vinylene units in the polymer backbone lead the absorption spectra to broaden and the photoluminescence emission spectra to red-shift in comparison to pristine polyfluorenes [9]. The structure is rigid and has a nearly one-dimensional coplanarity, which restrains the distortion of arylic rings, leading to high charge mobility. Thiophene and its derivatives have also been investigated as promising materials for optical devices, especially because of their narrow band gap and high stability [10]. Alkyl-substituted thiophenes, especially at position 3 of the aromatic ring, enable the preparation of regioregular polymers, which present interesting

* Corresponding author at: Laboratório de Nanotecnologia e Energia Solar (LNES), Universidade Estadual de Campinas (UNICAMP), Chemistry Institute, P.O. Box 6154, 13083-970 Campinas, SP, Brazil. Tel.: +55 19 35213029; fax: +55 193521 3023.
E-mail address: anaflavia@iqm.unicamp.br (A.F. Nogueira).

0379-6779/$ – see front matter © 2010 Elsevier B.V. All rights reserved.
doi:10.1016/j.synthmet.2010.05.036

optic and electronics properties [11,12] and high charge mobility [13].

The incorporation of thiophene units in polyfluorene systems can change the band gap, extending light-harvesting [10,14]. Thus, copolymers of these materials provide opportunities to attach different functional units so that the electronic and physical properties can be tuned according to the desired application. So far, copolymers containing fluorene and thiophene units directly linked by a single bond have been extensively investigated [15–21]. Research on materials containing these units linked by double bonds or vinylic groups, on the other hand, have not been well explored and only few reports can be found [22,23]. The presence of vinyl groups decreases the repulsion between aromatic hydrogens, thus leading to less twisting of the rings. In this work, new materials containing fluorene and thiophene units, linked by vinylene units (PPV-type polymers) are investigated and applied in organic solar cells.

2. Experimental

2.1. Photophysical and electrochemical measurements

UV–vis spectra were measured with a Cary 3G UV–vis spectrophotometer and fluorescence spectra were measured with a ISS Photon Counting Spectrofluorometer (excitation = 370 nm). Cyclic voltammetry was carried out in a conventional three electrode-cell (electrolyte: 0.1 mol L^{-1} of tetrabutylammonium tetrafluoroborate in anhydrous acetonitrile) with Ag/AgCl as reference electrode, a platinum wire as counter electrode and a polymer-coated platinum substrate (1 cm^2) as working electrode. Cyclic voltammograms were recorded at 30 mV s^{-1}, under nitrogen atmosphere, using an Eco Chemie Autolab PGSTAT 10 potentiostat. Film thickness and morphology were determined using a Veeco Nanoscope DI 3100 AFM microscope operating in the tapping mode. Molar mass determination was made by gel permeation chromatography (GPC) at a flow rate of 1 mL min^{-1} in THF on a Shimadzu Class-LC10 HPLC equipped with three Supelco Progel columns (G5000 + G4000 + G3000). The molar mass is reported relative to narrow dispersity polystyrene standards (2500, 5000, 17 500, 30 000, 50 000, 95 800 and 184 200).

2.2. Mobility measurements using the charge extraction by linearly increasing voltage (CELIV) method

Sandwich-type samples were prepared for charge carrier mobility measurements. The polymers were dissolved in chlorobenzene (20 mg/mL) and the solutions were filtered through a 0.45 μm PTFE filter before deposition by casting on top of pre-patterned ITO-covered glass substrates. The films were 200–400 nm thick. Subsequently, 30 nm aluminum top contacts were evaporated on top of the polymer (vacuum ~ 10^{-6} mbar). Samples were prepared under inert nitrogen atmosphere and the films were characterized in vacuum using an optical cryostat (Oxford Optistat DNV). For the CELIV experiments a variable pulse generator (Agilent 33250A) and oscilloscope (Tektronix TDS 754C) were used to record the current transients. To ensure the proper delay time between voltage and light pulse, a pulse and a function generators (Agilent AG33250A and Stanford DG535) were used. A frequency quadrupled Nd:YAG laser (Coherent Infinity 40–100) was employed to photogenerate the charge carriers using a 5 ns laser pulse at a wavelength of 355 nm and an intensity of less than 1 mJ/pulse. Carrier mobility was measured at an electric field of ~40 kV cm^{-1}.

2.3. Solar cells

Bulk-heterojunction solar cells were prepared according to the following procedure: indium tin oxide (ITO) coated glass substrates were cut to square pieces 1.5 cm × 1.5 cm and approximately half of ITO was chemically etched away. Substrates were then washed in an ultrasonic bath using acetone, isopropanol, ethanol and water, and dried under a nitrogen flow. A thin layer of poly(3,4-ethylenedioxythiophene)–poly(styrenesulfonate) (PEDOT:PSS) in aqueous solution (Baytron PH) was spin-coated on the substrates using 1500 rpm spin-coater speed, originating films of ~60 nm. Substrates covered with PEDOT were annealed on a hot plate for 10 min at 150 °C. The photoactive layer of polymer and [6,6]-phenyl C_{61}-butyric acid methyl ester (PCBM) was spin-coated on top from chlorobenzene solutions, using 800 rpm for 40 s, with typical thicknesses of 80–100 nm. To finalize the preparation of solar cell, the top electrode consisting of 0.7 nm LiF and subsequently 70 nm Al was evaporated in the vacuum (~10^{-6} mbar). The size of the active area of the solar cells was ~0.1 cm^2. During all measurements the samples were kept at room temperature. Later, the devices were thermally annealed on the hot plate at 130 °C for 10 min under nitrogen and measured again. A KHS Steuernagel solar simulator was adjusted to give 100 mW cm^{-2} of AM1.5G irradiation using a calibrated Si photodiode. Current–voltage curves were measured with a Keithley 236 source meter in the dark and under illumination. The incident-photon-to-electron conversion efficiency (IPCE) spectra were determined by shining light from a 75 W Xe lamp through an Acton monochromator and a chopper and measuring the resulting short-circuit current with an EG&G lock-in amplifier. Device fabrication and all electrical measurements were made in a nitrogen glove box to minimize degradation.

3. Results and discussion

Five different polymers containing fluorene, vinylene and thiophene and/or benzene units were synthesized through the Wittig route, originating alternate copolymers of poly(9,9-*n*-dihexyl-2,7-fluorenylenevinylene-*alt*-1,4-phenylenevinylene) (PF), poly(9,9-*n*-dihexyl-2,7-fluorenylenevinylene-*alt*-2,5-thienylenevinylene) (PFT), and copolymers with the combination of different ratios of these structures, as shown in Fig. 1. The synthesis of these materials can be found elsewhere [24,25]. The molar masses of these materials were determined using GPC (see supporting information). The values obtained are rather low: 9666, 4228, 3315, 14 363 and 7743 g mol^{-1} for PF, PF–PFT 75–25, PF–PFT 50–50, PF–PFT 25–75 and PFT, respectively. Conducting polymers usually present small chains, which frequently arise from the low solubility of the polymers in the solvents employed in the synthesis. Yu et al. [22] and Chen et al. [23] also synthesized conducting polymers containing fluorenylenevinylene and thienylenevinylene units, and obtained molar masses of about 15 000 and 42 000 g mol^{-1}, respectively. The values reported here are even lower than those reported by those authors, but in all cases the polymer chains can be considered small.

3.1. Photophysical and electrochemical properties

Thin film cyclic voltammetry was employed to investigate the electrochemical behavior of the conjugated polymers and to estimate the position of their highest occupied molecular orbital, HOMO (or valence band edge). For conducting polymers, the HOMO values can be estimated from the onset oxidation potentials measured in the voltammograms. This method is well accepted to estimate the energy levels of conjugated polymers [26–28]. Usually, the reduction potentials are not clearly seen for conducting poly-

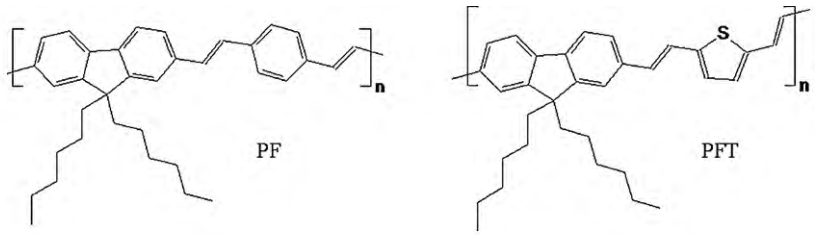

Polymers	PF	PFT
PF	100 %	-
PF-PFT 75-25	75 %	25 %
PF-PFT 50-50	50 %	50 %
PF-PFT 25-75	25 %	75 %
PFT	-	100 %

Fig. 1. Structure of the polymers investigated in this work.

mers. Therefore, one can estimate the LUMO (lowest unoccupied molecular orbital) position using the combination of the band gap energy (E_g) and HOMO values. The band gap can be estimated from the absorption spectra, using Tauc's equation [29]. Fig. 2 presents the values estimated for the polymers using this method. The values found for PCBM, ITO, PEDOT:PSS and aluminum are also shown.

The HOMO and LUMO values estimated for the polymers PF–PFT resemble the values obtained for the polymer PFT, suggesting that the presence of thiophene units dominated the characteristics. The values reported here are also similar to the values reported by other authors for polymers containing the combination of fluorene and thiophene units [23]. The polymer PF, on the other hand, presents very distinct characteristics, with higher values (less negative) for HOMO, LUMO and E_g.

Fig. 3 presents the absorption coefficient and the photoluminescence (PL) spectra obtained for polymer films deposited onto ITO-glass substrates. The absorption coefficient observed in Fig. 3a is very high in the region between 400 and 450 nm, reaching values comparable to those reported for other polymers, such as poly(3-alkylthiophene) (P3HT) [30] and poly[2-methoxy-5-(3,7-dimethyloctyloxy)-*p*-phenylene vinylene] (MDMO-PPV) [31]. As a general trend, the absorption coefficient increases with the increase in PF content. Also, PL intensity increases significantly with increasing in PF unit concentration, as can be seen in Fig. 3b. This could be related to the fact that, in the solid state, thiophene units tend to form strong interchain interactions, reducing the PL intensity [10]. Also, the heavy sulfur atoms can suppress singlet excitons, favor the formation of the triplet state and intersystem crossing, and therefore, reduce PL yield [32–34].

The maximum absorption and emission wavelengths are listed in Table 1. For comparison, the values of maximum absorption/emission wavelength reported for other polyfluorene and polythiophene derivatives are also shown.

The polymer containing only PF units present absorption maximum at ~400 nm (the PF characteristics are very similar to those

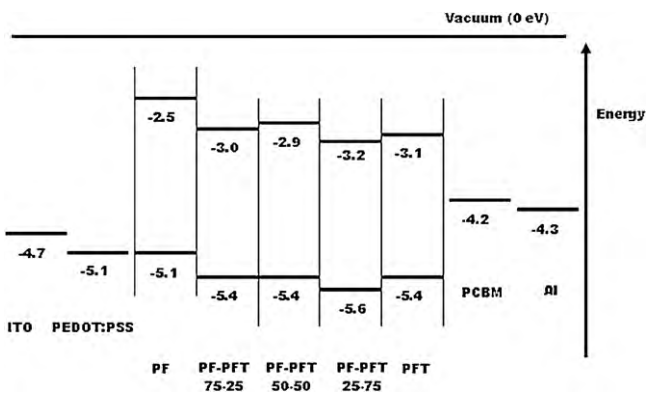

Fig. 2. Energy level diagram showing HOMO and LUMO levels for the polymers, LUMO of PCBM and the work function of the electrodes.

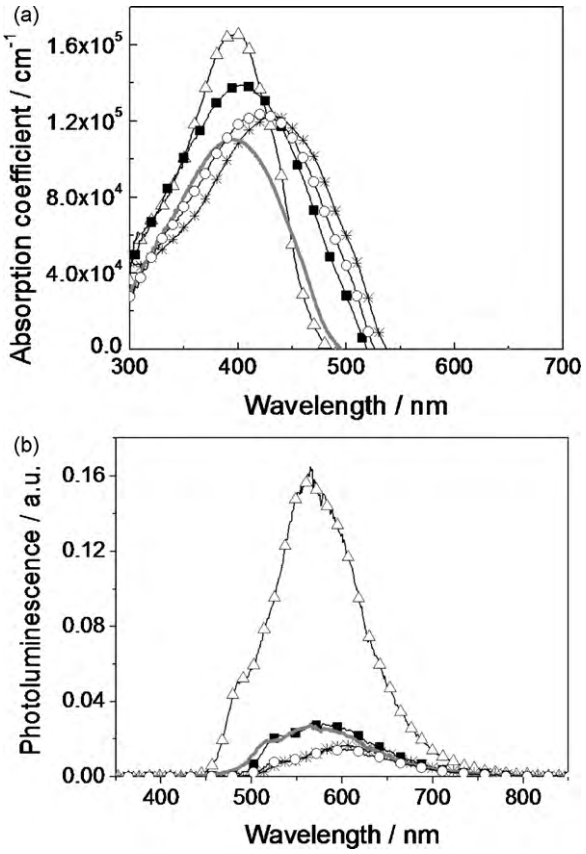

Fig. 3. Absorption coefficient (a) and photoluminescence (b) spectra obtained for polymer films of ~70–90 nm, deposited onto ITO-glass: (△) PF, (■) PF–PFT 75–25, (▬) PF–PFT 50–50, (○) PF–PFT 25–75 and (*) PFT.

Table 1
Absorption and emission (PL) maximum observed in the spectra of films of the polymers deposited onto ITO-glass. For comparison, values reported for polyfluorenes and poly(3-akyl-thiophene) derivatives are also shown [10,36].

Polymer	λ_{max} absorption (nm)	λ_{max} emission (nm)
PF	398	565
PF–PFT 75–25	405	580
PF–PFT 50–50	400	575
PF–PFT 25–75	420	605
PFT	430	605
Polyfluorenos[a]	350–410	410–500
Poly(3-alkyl-thiophene)s[b]	450–550	580–670

[a] From the work of Liu et al. [36].
[b] From the work of Perepichka et al. [10].

reported for polyfluorenes and/or polyfluorenylenevinylenes and are dominated by the presence of the fluorene unit [9,35]), while the polymer containing only PFT units presents absorption maximum at 430 nm. The copolymers containing both units present intermediate characteristics, indicating that the presence of thiophene units is indeed responsible to reduce the bandgap energy, as expected. On the other hand, these materials present significant absorption only in the region below 500 nm. As has been found for many other polymers based on thiophene units, absorption extended up to 600–750 nm would be desirable. The limited absorption observed for the materials investigated here is probably related to the small chain lengths observed for these polymers, which consist of about 10 repetitive units or less (see supporting information), in comparison with longer chains of commercially available P3HT, for example.

The polymers PF, PF–PFT 75–25 and PF–PFT 50–50 show PL maximum at 565, 580 and 575 nm, respectively, while the materials with higher thiophene concentrations (PFT and PF–PFT 25–75) show PL maximum at 605 nm. In both absorption and emission spectra, the polymer PF–PFT 50–50 presents an odd behavior, not following the expected trends. Its absorption and emission are blue-shifted and less strong (reduced PL intensity and absorption coefficient) than would be expected, compared with the polymers PF–PFT 75–25 and PF–PFT 25–75. This might be related to the very small chains in this polymer, with a average size of only 5 units per chain.

The results shown in Table 1 are similar to those reported by Yu et al. [22] for random copolymers of poly(fluorenylenevinylene) containing 10 or 20% of thienylenevinylene units. These authors show that there is energy transfer from the fluorene to thiophene units and, therefore, the later act as traps. Thus, the absorption characteristics are mainly influenced by the fluorenylenevinylene units, while the emission characteristics are dominated by the thienylenevinylene units. Energy transfers between fluorene and thiophene units have also been shown for other types of polymer structures [37,38].

3.2. Charge mobility

Dark current–voltage (J–V) curves were recorded for devices assembled with the different polymers, as shown in Fig. 4. These devices consisted of polymer films of ~70–90 nm sandwiched between PEDOT:PSS-covered ITO substrates and LiF/Al electrodes. A description by Vlegaar and collaborators for the J–V characteristics proposes that the behavior of PPV-based devices is dominated by the bulk conduction properties of the polymer, the hole current being governed by space charge limited conduction (SCLC) and the electron current being limited by the presence of traps [39,40]. Under the application of high positive bias, significant differences in the current density between the devices assembled with different polymers can be seen. The device assembled with PF is the one

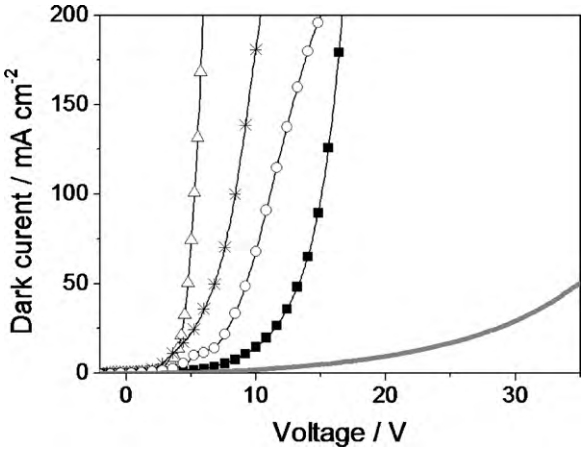

Fig. 4. J–V characteristics in the dark for devices with the following configuration: ITO | PEDOT:PSS | polymer | LiF | Al, where the polymer film thickness is about ~80–100 nm and the active area is ~0.1 cm^2. (△) PF, (■) PF–PFT 75–25, ( ) PF–PFT 50–50, (○) PF–PFT 25–75 and (*) PFT.

with the highest current and that assembled with PF–PFT 50–50 is the one with the lowest current. Higher current values can be attributed to two factors: increased equilibrium charge concentration, or increased charge mobility, according to Eq. (1), where J is the current density, q is the electron charge, e and p are the electron and hole concentrations, respectively, μ_e and μ_p are the electron and hole mobilities, respectively, and E is the electric field.

$$J = qe\mu_e E + qp\mu_p E \quad (1)$$

For an optimal performance of conjugated polymers in devices, sufficient charge carrier mobility is essential. Hence, to verify this ability for these materials, charge carrier mobility was measured using the charge carrier extraction by linearly increasing voltage (CELIV) technique. CELIV is a rather novel technique used to measure the carrier mobility in semiconductors with a broad range of conductivities, including conjugated polymers [41,42]. The advantage of this technique is that the carrier mobility can be directly measured from the experimentally recorded current transients and no data fitting procedures are required. Given the experimental conditions, the charge carrier mobility can be directly estimated from the extraction maximum of the current transient [43]. An additional advantage of CELIV is the possibility to estimate the mobility even when rather dispersive charge carrier transport prevails. Even though the carrier mobility and conductivity of the semiconducting materials can be measured in the dark, in the case of pure undoped organic semiconducting films, in which the sample conductivity is low, the charge carriers can also be generated using a laser pulse. The essence of this technique is that a triangular-shaped voltage pulse is applied to the sample. The initial current step (displacement current) is caused by the geometrical capacity of the film between the two electrodes. The increasing extraction current that follows is caused by the photoconductivity of the sample due to the photogenerated charge carriers. As the triangular voltage pulse continues to increase, electric field redistribution takes place inside the sample and carrier mobility values can be calculated directly from the current transients.

In Fig. 5a the experimental CELIV current transients typically obtained for the polymers investigated here are shown. The capacitive current response (black line in Fig. 5a) shows rather low equilibrium carrier concentrations in the film. In order to photogenerate additional charge carriers, a laser pulse was applied (photo-CELIV technique). The current transients are recorded for various delay times (t_{del}) between the laser pulse and the triangle-shaped voltage pulse. The extraction current transients (gray lines

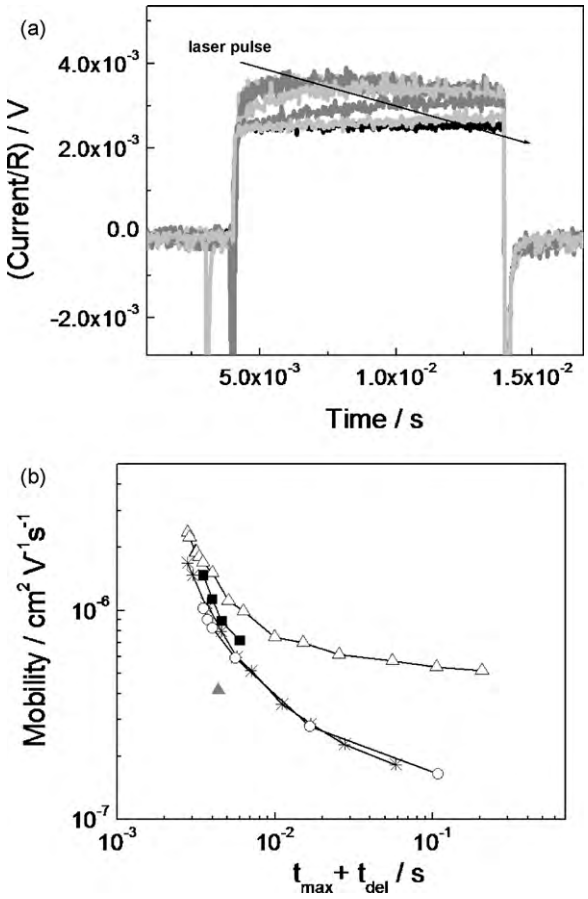

Fig. 5. Photo-CELIV current transients recorded for various delay times t_{del} between the laser pulse and the triangle-shaped voltage pulse (a) and charge carrier mobility calculated for the different polymers: (△) PF, (■) PF–PFT 75–25, (▲) PF–PFT 50–50, (○) PF–PFT 25–75 and (*) PFT.

in Fig. 5a, for different t_{del}) show rather dispersive extraction with an unpronounced extraction maximum, from which the charge carrier mobility is then estimated using Eq. (2), where A is the slope of the triangle-shaped voltage pulse, d is the film thickness and t_{max} is the time where the current reaches the maximum of extraction, observed in Fig. 5a.

$$\mu = \frac{2d^2}{3At_{max}^2} \quad (2)$$

The profile observed in Fig. 5a (unpronounced extraction maximum) suggests that the transport is dispersive, dominated by SCLC, due to disordered charge transport [44]. In Fig. 5b, the charge mobility is plotted as a function of time, which is the sum of both the delay time between the laser pulse and triangle-shaped voltage pulse and the extraction maximum. The quality of the PF–PFT 50–50 films was not good to allow reliable measurements. This is due to a frequent formation of pinholes in the film prepared by casting (see supporting information), which usually led to the observation of shorts. The carrier mobility for all polymers has a strong time-dependence which is attributed to the disordered nature of studied films, as well as to defects and traps in the bulk, caused either by the presence of impurities or inadequate, rough, heterogeneous and/or amorphous morphologies. At longer times, the carrier mobility approaches dynamic equilibrium and tends to saturation. The relaxation of the photogenerated charge carriers and the carrier mobility saturates when the density of states has a Gaussian distribution, as described by Bässler's theory of charge transport in disordered organic materials [44].

Table 2
Mobility values estimated using the CELIV technique.

Polymer	Mobility at 1 μs (10^{-6} cm^2 V^{-1} s^{-1})
PF	2.4
PF–PFT 75–25	1.5
PF–PFT 50–50	0.4
PF–PFT 25–75	1.0
PFT	1.7

In the CELIV experiments, the measured current is a sum of both faster and slower charge carrier mobilities, as shown in Eq. (1). However, for conducting polymers usually electron mobility is many orders of magnitude lower than hole mobility. Therefore, the measured mobility values can be attributed to the faster charge carriers [45], holes in this case. The motility values estimated at 1 μs after the laser pulse are presented in Table 2.

In this context it is noteworthy that the hole mobilities reported in the literature for MDMO-PPV using the CELIV technique are about 3×10^{-6} cm^2 V^{-1} s^{-1} [46], while the mobilities reported for P3HT and some polyfluorenes range from ~10^{-5} to ~10^{-2} cm^2 V^{-1} s^{-1}, depending on the measurement procedures utilized [47–49]. This demonstrates that hole mobility for unoptimized thin films of PF and PFT-based polymers are currently about the same order of magnitude of those of MDMO-PPV, but are about 2–3 orders of magnitude lower than those reported for P3HT, the most used polymer in organic solar cells.

According to Kline et al. [50], for regioregular-P3HT, the molar mass can also affect charge transport. For example, the field effect mobility measured by these authors changed from 1.7×10^{-6} to 9.4×10^{-3} cm^2 V^{-1} s^{-1} when the polymer molar mass is increased from 3.2 to 36.5 kDa. This effect was attributed to the formation of different morphologies (with different crystallite sizes and shapes) for polymers containing different molar masses. In the study presented here, the mobility values can also be related to the molar masses of the materials. The highest mobility values were obtained for PF and PFT, which present the highest molar masses. Also, all the polymeric materials present rather low mobility values, which might be related to the small chain sizes observed (consider that these materials are in fact oligomers, thus the film morphology might be affected by this parameter). Indeed, theoretical simulations using the Monte Carlo model predict a significant decrease in mobility for heterogeneous and full of defect-types of polymeric films [51]. Although in this work the degree of crystallinity of the polymers was not investigated, the work of Grova [24] and Chen et al. [23] showed that PFT and copolymers based on fluorene and thienylenevinylene units, respectively, are predominantly amorphous. These results suggest that this class of materials is not highly crystalline, as opposed to what is observed for P3HT.

The estimated mobility values are in agreement with the current density values observed under forward bias in the J–V curves in Fig. 4b: PF > PFT > PFT–PFT 25–75 > PF–PFT 75–25 > PF–PFT 50–50. Also, this sequence can be related to molar masses of the polymers: the polymers with higher molar masses also present the higher mobilities and current density values. This is probably related to the ability of higher-molar mass materials to assemble more defect-free and homogeneous films.

3.3. Solar cells

First, the PL spectra of polymer films after mixing with 50 wt% of PCBM were obtained (see supporting information). An almost complete quenching of the polymer emission was observed, which can be considered as a first indication of the existence of charge transfer between the polymer and PCBM. Then, devices were assembled by adding 50 or 80 wt% of PCBM to the polymers. The ideal concentration of PCBM is different for each system, as it strongly depends

Table 3
Photovoltaic parameters obtained for solar cells assembled with polymer + PCBM (active area ~ 0.1 cm^2), illuminated under 100 mW cm^{-2}: short-circuit current (J_{sc}), open circuit voltage (V_{oc}) and fill factor (FF). The values presented correspond to the mean and standard deviation after 12 measurements.

Polymer	PCBM (wt%)	J_{sc} (mA cm^{-2})	V_{oc} (V)	FF (%)
PF	50	0.12 ± 0.02	0.18 ± 0.02	27 ± 1
PF–PFT 75–25	50	0.20 ± 0.04	0.40 ± 0.01	28 ± 2
PF–PFT 50–50	50	0.51 ± 0.05	0.38 ± 0.04	29 ± 2
PF–PFT 25–75	50	0.78 ± 0.04	0.67 ± 0.03	25 ± 1
PFT	50	0.72 ± 0.04	0.48 ± 0.02	27 ± 1
PF	80	0.22 ± 0.02	0.35 ± 0.05	27 ± 2
PF–PFT 75–25	80	1.0 ± 0.4	0.50 ± 0.03	27 ± 2
PF–PFT 50–50	80	1.1 ± 0.4	0.53 ± 0.02	27 ± 2
PF–PFT 25–75	80	2.4 ± 0.3	0.64 ± 0.02	28 ± 1
PFT	80	1.6 ± 0.3	0.58 ± 0.03	28 ± 3
MDMO-PPV	80	3 ± 1	0.65 ± 0.08	40 ± 4
P3HT	50	10 ± 2	0.60 ± 0.02	53 ± 2

on the morphology, phase separation and formation of crystallites. For example, when using P3HT, the ideal concentration of PCBM is around 30–50 wt%, while for MDMO-PPV it is ~80% [52,53] and for polyfluorene it is ~75% [54]. For poly(thienylenevinylene), Smith et al. [55] showed that the use of PCBM concentrations above 80% enhances the photocurrent and efficiency of the devices.

Table 3 presents the parameters extracted from *J–V* curves for devices operating under 100 mW cm^{-2} of white light illumination. Three devices of each kind were measured, where each of them consisted of four different electric contacts. Thus, the values reported in Table 3 shows the mean and standard deviation obtained after 12 measurements. The deviation values are included because they denote the reproducibility of the devices. For comparison, the values obtained for devices assembled and characterized in the same conditions, using MDMO-PPV or P3HT as hole conduction materials, are also shown.

For all polymers investigated, both the short-circuit current (J_{sc}) and the open circuit voltage (V_{oc}) increase when the amount of PCBM is increased. This behavior is similar to that observed for MDMO-PPV, which would be expected, since the materials investigated here present PPV-type structures.

In this kind of device, it is accepted that the thermodynamic limit for V_{oc} is given by the energetic difference between the LUMO of PCBM (−4.2 eV) and the HOMO of the polymer [56]. For MDMO-PPV and P3HT, the estimated HOMO values are −5.3 and −5.2 eV, respectively [57,58]. The polymers investigated here present similar HOMO values (see Fig. 2), reflecting in satisfactory V_{oc} values for the devices assembled, as can be seen in Table 3. The exception is the device assembled with PF, which shows lower V_{oc}, due to the less negative value of the HOMO of this material.

The analysis of J_{sc} is not straightforward. There must be a balance between at least two distinct effects: improved light-harvesting and improved charge transport and collection. The higher mobility is responsible for a better transport of free charge carriers to the electrodes, while the improved light-harvesting allows the generation of more excitons, which can provide the generation of more free charge carriers. Both effects contribute to increase J_{sc}. It is also important to notice that morphology plays a crucial role, since an extended interface must be formed between the polymer and PCBM to allow an efficient dissociation of excitons into free charge carriers, and at the same time a percolation network must exist in each phase, to allow the efficient transport of charge carriers [59].

For the assembled devices, the lowest J_{sc} are observed for PF, despite the higher charge carrier mobility presented by this polymer. In this case, the low J_{sc} is attributed to the poor light absorption shown by this material. It is interesting to notice that devices prepared with PF–PFT 50–50 delivered higher J_{sc} compared to devices assembled with PF, despite the fact that both materials have similar light-absorption characteristics. This might arise from a better interaction of PF–PFT 50–50 with PCBM, and the formation of

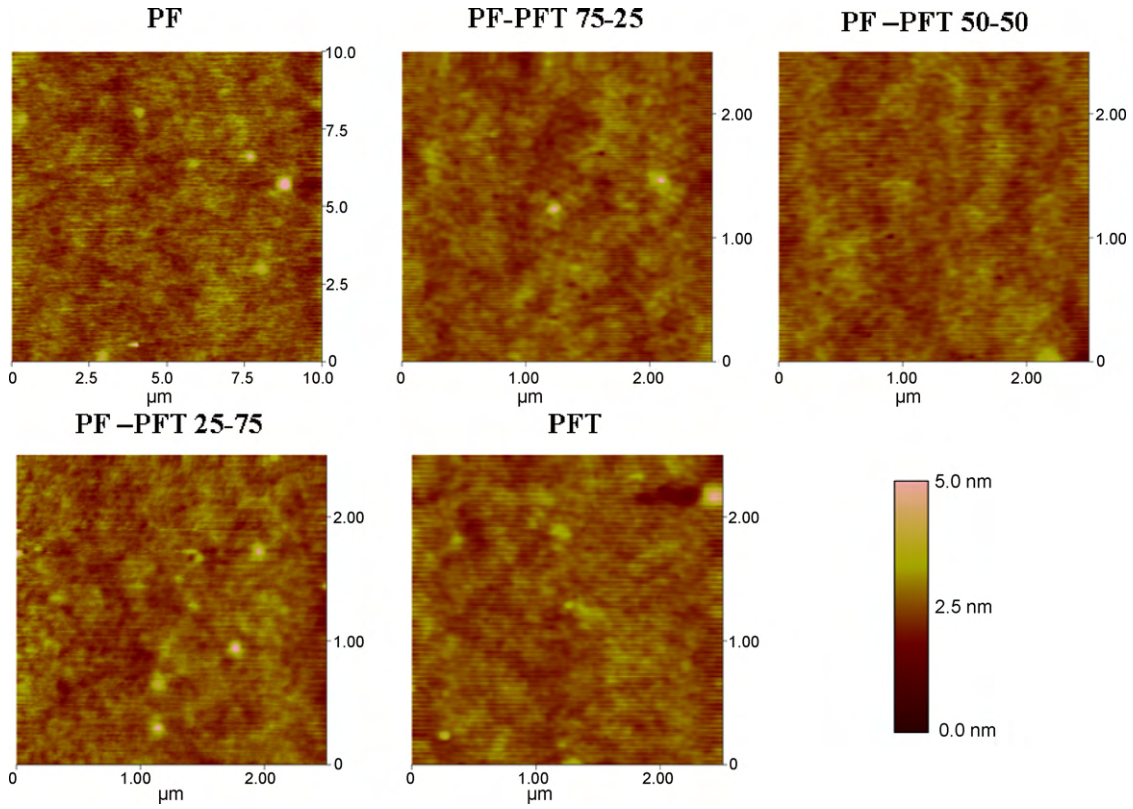

Fig. 6. Tapping mode AFM of films of different polymers mixed with 80 wt% of PCBM. The scanning area is 2.5 μm × 2.5 μm.

Table 4
Photovoltaic parameters obtained for solar cells assembled with polymer + PCBM after annealing at 130 °C for 5 min, illuminated under 100 mW cm^{-2} (active area ~ 0.1 cm^2): short-circuit current (J_{sc}), open circuit voltage (V_{oc}) and fill factor (FF).

Polymer	PCBM (wt%)	J_{sc} (mA cm^{-2})	V_{oc} (V)	FF (%)
PF	80	0.1	0.30	28
PF–PFT 75–25	80	1.3	0.45	33
PF–PFT 50–50	80	1.0	0.50	35
PF–PFT 25–75	80	2.0	0.60	35
PFT	80	0.9	0.55	28

a more appropriate morphology in the films prepared by spin-coating.

Besides, although PFT is the material which presented the best light-harvesting, and the second highest charge mobility, the best photovoltaic devices were obtained using the copolymer PF–PFT 25–75. This is probably related to the existence of a synergistic effect between PF and PFT units in this material: PF units show higher emission, and have a more rigid structure, which can account for better charge transport; on the other hand, PFT units might deactivate singlet excitons, but their presence decreases the bandgap energy of the material, contributing to improve light-harvesting. It is also possible that, somehow, the coexistence of these units in one material may lead to the formation of a better morphology, maximizing the interface for exciton splitting, while maintaining the percolation network.

Even after optimization of the PCBM concentration, the observed fill factor (FF) values are still low (~30%, while for solar cells assembled with MDMO-PPV the values are above 50% [8,60]). The low FF values indicate the existence of recombination losses, caused by poor charge transport or by film morphology. Even though the mobility values reported here are quite low, they are on the same order of magnitude of those reported for MDMO-PPV. Therefore, the lower FF values may result from morphology. To investigate this parameter, AFM images for polymer–PCBM mixtures deposited by spin-coating are shown in Fig. 6. The films are rather smooth, homogeneous, with few – if any – defects, revealing a good mixing between the materials. As shown in other works, there should be phase separation, at least to a certain extent, with the formation of PCBM-rich and polymer-rich domains, which can improve the charge transport properties while maintaining the interface for exciton splitting [61–63].

Next, an annealing treatment was applied to the devices (130 °C for 5 min), in order to investigate if this could allow for a better organization of polymer chains and PCBM domains in the film, thus changing the morphology and improving FF. This effect is commonly observed for P3HT based devices, and also increases the J_{sc} values [30,62,63]. For MDMO-PPV-based devices, on the other hand, depending on the solvent from which the films are deposited, it is known that annealing may lead to a pronounced phase separation, with formation of too large aggregates of PCBM, resulting in losses in charge transport [61].

Fig. 7a presents the *J–V* characteristics for the annealed devices. The parameters extracted from these curves are listed in Table 4. Fig. 7b shows the IPCE characteristics for devices assembled with 80 wt% of PCBM. As a general trend, the IPCE profile follows the polymer absorption spectra profile.

For PF and PFT a decrease in both V_{oc} and J_{sc}, with no improvements in FF, is observed. These materials present a similar behavior as observed for PCBM/MDMO-PPV cast from toluene solutions, where the annealing also led to excessive phase separation, resulting in less current collection and lower V_{oc}. For the PF–PFT copolymers, independent of the ratio of PF and PFT units, the FF values increased, and J_{sc} and V_{oc} are almost unaffected by the heat

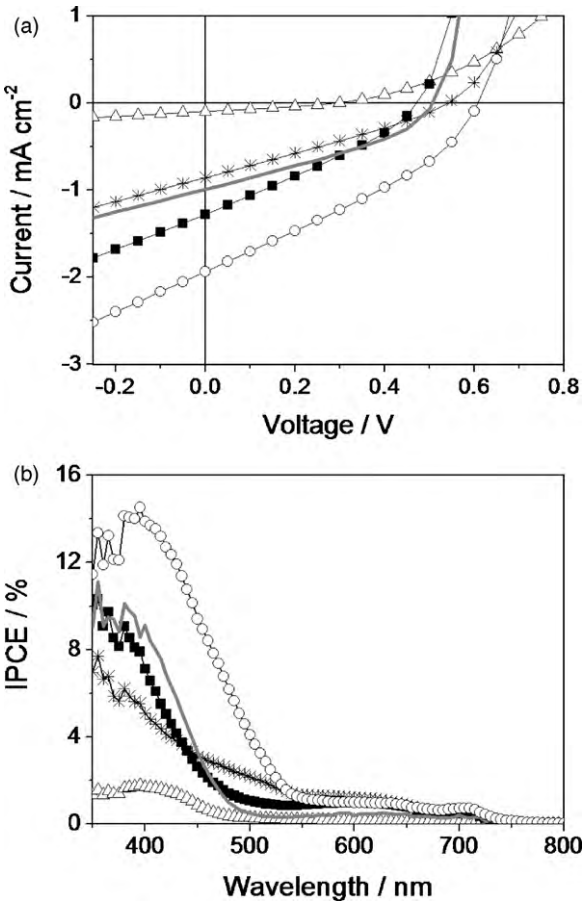

Fig. 7. *J–V* curves under 100 mW cm^{-2} (a) and IPCE characteristics (b) for devices assembled with 80 wt% of PCBM, ~0.1 cm^2 active area, annealed at 130 °C for 5 min: (△) PF, (■) PF–PFT 75–25, (▬) PF–PFT 50–50, (○) PF–PFT 25–75 and (*) PFT.

treatment. In these samples, the improved FF must arise from an improved contact with the aluminum electrode. The smaller chain size in these polymers may facilitate rearrangements in the film surface, allowing the formation of a better contact at the interface. Nevertheless, all the FF values measured in this work are still low. Since this was attributed to morphology effects, some alternatives to improve this parameter would be the use of polymers with higher molar mass (longer chains), or the introduction of a third component in the active layer, such as CdSe nanoparticles, which can change the morphology, resulting in more efficient devices, as will be reported elsewhere [64].

4. Conclusions

In this work, the electrochemical, photophysical and charge mobility properties of new PPV-type polymeric materials, based on the combination of fluorene and thiophene units, were investigated. These materials were also used to assemble organic solar cells, in combination with the fullerene derivative PCBM. Light-harvesting and charge transport measured for these materials (~10^{-6} cm^2 V^{-1} s^{-1}) are low compared to the characteristics of the commercially available polymer P3HT. The *J–V* results showed that the fill factor was low, but the current and voltage values obtained for devices based on PFT and PF–PFT 25–75 were comparable to those obtained for devices assembled with MDMO-PPV. The voltages are similar to or higher than those obtained when using P3HT, but the current is still much lower compared to this polymer. It was also evident that the molar mass (chain size) of these materials must be increased, in order to improve light absorption, charge

transport, and film morphology, which are crucial for the assembly of high efficiency solar cells.

Acknowledgments

The authors thank CNPq, INEO and Fapesp (fellowship 05/56924-0) for financial support. We also thank Prof. Carol Collins for English revision.

Appendix A. Supplementary data

Supplementary data associated with this article can be found, in the online version, at doi:10.1016/j.synthmet.2010.05.036.

References

[1] J.Y. Kim, K. Lee, N.E. Coates, D. Moses, T.-Q. Nguyen, M. Dante, A.J. Heeger, Science 317 (2007) 222.
[2] A. Privikas, P. Stadler, H. Neugebauer, N.S. Sariciftci, Org. Electron. 9 (2008) 775.
[3] B.R. Saunders, M.L. Turner, Adv. Colloid Interface Sci. 138 (2008) 1.
[4] T. Ameri, G. Dennler, C. Lungenschmied, C.J. Brabec, Energy Environ. Sci. 2 (2009) 347.
[5] M. Helgesen, R. Sondergaard, F.C. Krebs, J. Mater. Chem. 20 (2010) 36.
[6] L. Akcelrud, Prog. Polym. Sci. 28 (2003) 875.
[7] T. Stübinger, W. Brütting, J. Appl. Phys. 90 (2001) 3633.
[8] S.E. Shaheen, C.J. Brabec, N.S. Sariciftci, F. Padinger, T. Fromherz, J.C. Hummelen, Appl. Phys. Lett. 78 (2001) 841.
[9] S.-H. Jin, H.-J. Park, J.Y. Kim, K. Lee, S.-P. Lee, D.-K. Moon, H.-J. Lee, Y.-S. Gal, Macromolecules 35 (2002) 7532.
[10] I.F. Perepichka, D.F. Perepichka, H. Meng, F. Wudl, Adv. Mater. 17 (2005) 2281.
[11] K. Faid, M. Fréchette, M. Ranger, L. Mazerolle, I. Lévesque, M. Leclerc, Chem. Mater. 7 (1995) 1390.
[12] R.M.S. Maior, K. Hinkelmann, H. Eckert, F. Wudl, Macromolecules 23 (1990) 1268.
[13] R.D. McCullough, S. Tritsram-Nagle, S.P. Williams, R.D. Lowe, M. Jayaraman, J. Am. Chem. Soc. 115 (1993) 4910.
[14] W.J. Mitchell, C. Pena, P.L. Burn, J. Mater. Chem. 12 (2002) 200.
[15] B. Liu, Y.-H. Niu, W.-L. Yu, Y. Cao, W. Huang, Synth. Met. 129 (2002) 129.
[16] B. Liu, W.-L. Yu, Y.-H. Lai, W. Huang, Macromolecules 33 (2000) 8945.
[17] A. Donat-Bouillud, I. Lévesque, Y. Tao, M. D'Iorio, Chem. Mater. 12 (2000) 1931.
[18] S. Beaupré, M. Leclerc, Adv. Funct. Mater. 12 (2002) 192.
[19] R.A. Street, A. Salleo, M. Chabinyc, K. Paul, J. Non-Cryst. Solids 338–340 (2004) 607.
[20] U. Asawapirom, R. Guntner, M. Forster, U. Scherf, Thin Solid Films 477 (2005) 48.
[21] W. Tang, L. Ke, L. Tan, T. Lin, T. Kietzke, Z.-K. Chen, Macromolecules 40 (2007) 6164.
[22] N. Yu, R. Zhu, B. Peng, W. Huang, W. Wei, J. Appl. Polym. Sci. 108 (2008) 2438.
[23] B. Chen, Y. Wu, M. Wang, S. Wang, S. Sheng, W. Zhu, R. Sun, H. Tian, Eur. Polym. J. 40 (2004) 1183.
[24] I.R. Grova, Synthesis and electro-optical characterization of poly(9,9′-n-hexyl-2,7-fluorene-diil-vinylene-2,5-thiophene), Master thesis, Universidade Federal do Paraná, Brazil, 2007;
A. Glogauer, Synthesis and photophysical characterization of two electroluminescent copolymers, one conjugated and one multiblock using fluorene–vinylene–fluorene as chromophore, Master thesis, Universidade Federal do Paraná, Brazil, 2004.
[25] L.C. Akcelrud et al., unpublished results.
[26] H. Eckhardt, L.W. Shacklette, K.Y. Jen, R.L. Elsenbaumer, J. Chem. Phys. 91 (1989) 1303.
[27] Y.F. Li, Y. Cao, J. Gao, D.L. Wang, G. Yu, A.J. Heeger, Synth. Met. 99 (1999) 243.
[28] Q.J. Sun, H.Q. Wang, C.H. Yang, Y.F. Li, J. Mater. Chem. 13 (2003) 800.
[29] D.L. Wood, J. Tauc, Phys. Rev. B 5 (1972) 3144.
[30] H. Hoppe, N.S. Sariciftci, J. Mater. Res. 19 (2004) 1924.
[31] H. Hoppe, N. Arnold, N.S. Sarciftci, D. Meissner, Sol. Energy Mater. Sol. Cells 80 (2003) 105.
[32] H. Saadeh, T. Goodson, L. Yu, Macromolecules 30 (1997) 4608.
[33] B. Kraabel, D. Moses, A.J. Heeger, J. Chem. Phys. 103 (1995) 5102.
[34] D. Beljonne, Z. Shuai, G. Pourtois, J.-L. Bredas, J. Phys. Chem. A 105 (2001) 3899.
[35] G. Klaerner, R.D. Miller, Macromolecules 31 (1998) 2007.
[36] B. Liu, W.-L. Yu, Y.-H. Lai, W. Huang, Chem. Mater. 13 (2001) 1984.
[37] G. Vamvounis, G.L. Schulz, S. Holdcroft, Macromolecules 37 (2004) 8897.
[38] G. Vamvounis, S. Holdcroft, Adv. Mater. 16 (2004) 716.
[39] P.W.M. Blom, M.J. de Jong, J.J.M. Vlegaar, Appl. Phys. Lett. 68 (1996) 3308.
[40] P.W.M. Blom, M.J.M. de Jong, C.T.H.F. Liedenbaum, J.J.M. Vlegaar, Synth. Met. 85 (1997) 1287.
[41] G. Juska, K. Arlauskas, M. Viliunas, K. Genevicius, R. Österbacka, H. Stubb, Phys. Rev. B 62 (2000) R16235.
[42] K. Genevicius, R. Österbacka, G. Juska, K. Arlauskas, H. Stubb, Thin Solid Films 403 (2002) 415.
[43] R. Osterbacka, A. Pivrikas, G. Juska, K. Genevicius, K. Arlauskas, H. Stubb, Curr. Appl. Phys. 4 (2004) 534.
[44] H. Bässler, Phys. Status Solidi B 175 (1993) 15.
[45] G. Juska, K. Genevicius, G. Sliauzys, A. Pivrikas, M. Scharber, R. Österbacka, J. Appl. Phys. 101 (2007) 114505.
[46] G. Dennler, A.J. Mozer, G. Juska, A. Pivrikas, R. Osterbacka, A. Fucnsbauer, N.S. Sariciftci, Org. Electron. 7 (2006) 229.
[47] L. Bozano, S.A. Carter, J.C. Scott, G.G. Malliaras, P.J. Brock, Appl. Phys. Lett. 74 (1999) 1132.
[48] S.A. Choulis, J. Nelson, Y. Kim, D. Poplavsky, T. Kreouzis, J.R. Durrant, D.D.C. Bradley, Appl. Phys. Lett. 83 (2003) 3812.
[49] A.J. Mozer, N.S. Sariciftci, A. Pivrikas, R. Osterbacka, G. Juska, L. Brassat, H. Basller, Phys. Rev. B 71 (2005) 035214.
[50] R.J. Kline, M.D. McGehee, E.N. Kadnikova, J. Liu, J.M.J. Fréchet, Adv. Mater. 15 (2003) 1519.
[51] C. Groves, L.J.A. Koster, N.C. Greenham, J. Appl. Phys. 105 (2009) 094510.
[52] C. Müller, T.A.M. Ferenczi, M. Campoy-Quiles, J.M. Frost, D.D.C. Bradley, P. Smith, N. Stingelin-Stutzmann, J. Nelson, Adv. Mater. 20 (2008) 3510.
[53] J.K.J. van Duren, X. Yang, J. Loos, C.W.T. Bulle-Lieuwma, A.B. Sieval, J.C. Hummelen, R.A.J. Janssen, Adv. Funct. Mater. 14 (2004) 425.
[54] R. Pacios, D.D.C. Bradley, J. Nelson, C.J. Brabec, Synth. Met. 137 (2003) 1469.
[55] A.P. Smith, R.R. Smith, B.E. Taylor, M.F. Durstock, Chem. Mater. 16 (2004) 4687.
[56] C.J. Brabec, A. Cravino, D. Meissner, N.S. Sariciftci, T. Fromherz, M.T. Rispens, L. Sanchez, J.C. Hummelen, Adv. Funct. Mater. 11 (2001) 374.
[57] D. Mühlbacher, H. Neugebauer, A. Cravino, N.S. Sariciftci, J.K.J. van Duren, A. Dhanabalen, P.A. van Hal, R.A.J. Jansen, J.C. Hummelen, Mol. Cryst. Liq. Cryst. 385 (2002) 205.
[58] M. Onoda, K. Tatda, A.A. Zakhidov, K. Yoshino, Thin Solid Films 331 (1998) 76.
[59] H. Hoppe, T. Glatzel, M. Niggemann, W. Schwinger, F. Schaeffler, A. Hinsch, M.Ch. Lux-Steiner, N.S. Sariciftci, Thin Solid Films 511–512 (2006) 587.
[60] C.J. Brabec, N.S. Sariciftci, J.C. Hummelen, Adv. Funct. Mater. 11 (2001) 15.
[61] H. Hoppe, M. Niggemann, C. Winder, J. Kraut, R. Hiesgen, A. Hinsch, D. Meissner, N.S. Sariciftci, Adv. Funct. Mater. 14 (2004) 1005.
[62] H. Hoppe, N.S. Sariciftci, J. Mater. Chem. 16 (2006) 45.
[63] X. Yang, J. Loos, S.C. Veenstra, W.J.H. Verhees, M.M. Wienk, J.M. Kroon, M.A.J. Michels, R.A.J. Janssen, Nano Lett. 5 (2005) 579.
[64] J.N. de Freitas, I.R. Grova, L.C. Akcelrud, N.S. Sariciftci, A.F. Nogueira, J. Mater. Chem. 20 (2010) 4845.